Transient evolution regimes in a multiscale dynamo model: Timescales of the reversal mechanism

C. Narteau[1]
Grant Institute, School of Geosciences, University of Edinburgh, Edinburgh, UK

J. L. Le Mouël
Laboratoire de Géomagnétisme, Institut de Physique du Globe de Paris, Paris, France

Received 20 January 2004; revised 29 October 2004; accepted 11 November 2004; published 20 January 2005.

[1] In order to better understand the origin and nature of reversals of the Earth's magnetic field, we examine the reversal mechanism of a multiscale dynamo model. This model can be described as a cellular automaton with long-range interaction. Different states correspond to different types of helical motions, and a hierarchical structure of length scales is used to mimic helicity transfers in fully developed turbulence. These multiscale helical motions and a differential rotation are the ingredients of a schematic $\alpha\omega$ dynamo. The model exhibits rich behavior, including long periods of stable magnetic polarity (i.e., chrons), sudden reversals, excursions, and secular variation. Three transient regimes of evolution emerge: (1) Chrons are initiated by an amplification mechanism, which involves spontaneous reorientation of large length scale circulation and an α-quenching mechanism reinforcing the asymmetry of flow during runaway growth in magnetic field intensity. (2) During the chrons the injection of turbulence at small length scale slowly restores the symmetry of the system and leads to reversal. (3) During reversals the magnetic field does not remember its previous polarity, its intensity collapses, and spontaneous reorientation of large length scale circulation is more likely to occur (see regime 1). Reversal duration therefore corresponds to an upper value of the time constants for underlying turbulence in the absence of a magnetic field. We observe a constant excursion rate during chrons and a power law relationship between the reversal rate and the magnitude of helical forcing until a limit for dynamo action is reached. Extrapolated to the Earth's dipole field, this model predicts the duration of both chrons and reversals and sheds light on physical processes that may be responsible for their systematic occurrence.

Citation: Narteau, C., and J. L. Le Mouël (2005), Transient evolution regimes in a multiscale dynamo model: Timescales of the reversal mechanism, *J. Geophys. Res.*, *110*, B01104, doi:10.1029/2004JB002983.

1. Introduction

[2] Recent numerical simulations and laboratory experiments have buttressed the hypothesis that large-scale magnetic fields may be generated and sustained by the interplay between mechanical and electromagnetic processes inside planetary bodies [*Glatzmaier and Roberts*, 1995a, 1995b; *Kageyama and Sato*, 1997; *Kuang and Bloxham*, 1997; *Olson et al.*, 1999; *Gailitis et al.*, 2000; *Tilgner*, 2000]. This so-called dynamo mechanism requires an electrically conductive liquid, rapid rotation, and sources of thermal or compositional buoyancy to maintain convection. As the fluid rises or sinks, Earth's rotation may produce helical motions, which shear the preexisting magnetic field. This shearing creates a secondary magnetic field as the preexisting magnetic field diffuses. Conversely, the electric and magnetic fields affect the fluid's motions through electrodynamic forces. The fully developed case of a magnetohydrodynamics (MHD) geodynamo is an extremely difficult problem to tackle because of numerical limitations at very small Ekman number $E = \nu/\Omega d^2$ (ν is the kinematic viscosity, Ω is the Earth (planet) rotation, and d is a characteristic length of the core). Indeed, in the outer core of the Earth, the viscosity is quite low ($\nu \approx 10^{-6}$ m^2 s^{-1}), and turbulent motions are likely to exist over a wide range of spatial scales. On the other hand, high magnetic diffusivity of the liquid iron alloy may promote a large-scale magnetic field through the inhibition of its small-scale structures.

[3] Paleomagnetic and geomagnetic data provide, over different timescales, a unique set of information on the dynamo mechanism acting in the Earth's liquid outer core. When averaged over several thousand years, these data reveal that the internal geomagnetic field is essentially

[1]Now at Laboratoire de Géomagnériaux, Institut de Physique du Globe de Paris, Paris, France.

0148-0227/05/2004JB002983$09.00

dipolar and that the orientation of the dipole is close to the Earth's rotation axis. The polarity of the dipole changes over geological timescales, and the duration of the reversals is much shorter than the periods of constant polarity (chrons). In fact, during the last 10^7 years, chrons had an average duration of 2×10^5 years [*Merrill et al.*, 1996]. Reversals, on the other hand, may last fewer than 5×10^3 years [*Quidelleur*, 2003]. During a reversal, the intensity of the dipole field is decreased [*Valet*, 2003]; the details of the process are still subject to controversy, given the relative importance of the nondipole components of the magnetic field in these periods. During chrons, sudden and abrupt changes in the intensity and orientation of the dipolar magnetic field are called excursions, while smaller and more frequent fluctuations of the dipole intensity constitute its so-called secular variation [*Guyodo and Valet*, 1999]. Superimposed on these variations, a permanent decrease in dipole field intensity yields the saw-tooth pattern often observed between two reversals in paleomagnetic records [*Valet and Meynadier*, 1993]. Over tens of millions years, the reversal rate may significantly change. Two major observations are (1) the occurrence of superchrons, i.e., extremely long periods of time without polarity reversal, and (2) the increase in the reversal rate since the end of the last superchron, 83×10^6 years ago (average chron duration is estimated to have decreased by a factor of nearly 5 [*Cande and Kent*, 1995]).

[4] Despite significant progress in geodynamo studies, we do not yet have a full understanding of reversals within the overall dynamo mechanism. Different types of modeling techniques can be explored. Systematic three-dimensional (3-D) simulation of magnetohydrodynamics interactions may be the most promising method; nevertheless, computer technology still needs to improve considerably [*Zhang and Schubert*, 2000; *Dormy et al.*, 2000]. Furthermore, new obstacles to a complete modeling of the geodynamo may appear, as is presently the case in the analysis of thermal convection at high Rayleigh number [*Kadanoff*, 2001].

[5] At the present time, other techniques can also be used to contribute to a better understanding of the geodynamo mechanism and its reversals. One is to study disc dynamo and equivalent systems [*Bullard*, 1955; *Rikitake*, 1958; *Hide*, 1995]. A second is to develop $\alpha\omega$ dynamos [*Braginsky and Roberts*, 1987; *Hollerbach et al.*, 1992; *Jault*, 1995] in which a mean helicity and large-scale differential rotation are the ingredients by which poloidal (α effect) and toroidal (ω effect) fields are mutually generated [*Moffatt*, 1978; *Krause and Rädler*, 1980]. A third way is to analyze the dynamo as a nonlinear dynamical system. For example, *Hoyng et al.* [2001] study the geodynamo as a bistable oscillator; the basic equations contain the same ingredients as the model presented here, as according to *Le Mouël et al.* [1997]. Nevertheless, the models of turbulence differ in nature. As in classical $\alpha\omega$ dynamos, *Hoyng et al.* [2001] used a predetermined α effect with a simplified quenching mechanism inversely proportional to the intensity of the magnetic energy. In contrast, the originality of our approach lies primarily in the fact that mean helicity is not determined a priori, but results from a model of turbulence in which the evolution of multiscale helical motions is controlled by the intensity of the magnetic energy. As a result, reversals may occur in an $\alpha\omega$ dynamo as well as an α^2 dynamo in which both poloidal and toroidal fields are mutually generated through the α effect.

[6] We investigated magnetic field phenomenology with a numerical dynamo model inspired by recent developments in statistical physics. It is well established in the field that short-range interactions may lead to macroscopic behavior [*Bak*, 1997] and that a mechanism of emergence may relate micro and macro levels of description (see section 3.2.2). A key aspect of our method is to introduce a criterion based on local flow and another one based on local electromagnetic coupling between cyclonic motions and the large-scale magnetic field. In addition, we consider that a hierarchical structure of length scales accounts for the nature of turbulent thermal convection at very high Rayleigh number. Interactions between constituent parts of the system at different length scales mimic the cascades in turbulent flow, i.e., the transfer of a physical quantity over a wide range of length scales. Change in magnetic field intensity is governed by a set of coupled differential equations, and the magnitude of the magnetic energy affects the characteristic timescale of the cascades.

2. The Model

[7] The multiscale dynamo model has previously been described by *Narteau et al.* [2000], who present a more complete description than the brief summary below is presented.

2.1. Schematic Equations of a $\alpha\omega$ Dynamo

[8] We break down the magnetic field, $\mathbf{B}$, into poloidal, $\mathbf{B}_S$, and toroidal, $\mathbf{B}_T$, ingredients,

$$\mathbf{B} = \mathbf{B}_S + \mathbf{B}_T, \tag{1}$$

where each of these ingredients is the product of a space function and a time function

$$\mathbf{B}_T(\mathbf{r}, t) = T(t)\boldsymbol{\mathcal{B}}_T(\mathbf{r}) \tag{2}$$

$$\mathbf{B}_S(\mathbf{r}, t) = S(t)\boldsymbol{\mathcal{B}}_S(\mathbf{r}), \tag{3}$$

where $\mathbf{r}$ is the current point and t time. Thus we only consider a single mode of both the toroidal and poloidal fields. For example, $\boldsymbol{\mathcal{B}}_S(\mathbf{r})$ can be the poloidal mode $\mathbf{P}_1^0$ and $\boldsymbol{\mathcal{B}}_T(\mathbf{r})$ can be the toroidal mode $\mathbf{T}_2^0$. $S(t)$ may then be directly related to both the intensity and the polarity of the geomagnetic dipole.

[9] We consider an $\alpha\omega$ dynamo mechanism in which toroidal is generated from the poloidal field through differential rotation, and the poloidal is generated from the toroidal field through the shearing of the magnetic field by helical motions [*Moffatt*, 1978; *Krause and Rädler*, 1980]. Secondary magnetic fields may then increase in intensity while preexisting fields are diffusing. Hence we consider

$$\frac{\partial T(t)}{\partial t} + K_T T(t) = \omega S(t) \tag{4}$$

$$\frac{\partial S(t)}{\partial t} + K_S S(t) = \mathcal{H}(t) T(t), \tag{5}$$

where ω is the differential rotation, $\mathcal{H}(t)$ is a parameter representative of the mean helicity at time t (see equation (6)), and K_S^{-1} and K_T^{-1} are the diffusive times for the poloidal and toroidal fields, respectively [*Le Mouël et al.*, 1997]. We will take $K_S = K_T = K = 10^{-4}$ yr^{-1} and $\omega = 2 \times 10^{-4}$ yr^{-1}.

[10] Although system (4)–(5) resembles a classical system of two linear coupled first-order differential equations, it is not. Its interest derives from the nonlinear term $\mathcal{H}(t)$. At a given time t, $\mathcal{H}(t)$ depends on the history of the dynamo mechanism before t. Nonetheless, some of the reasoning valid for the linear system (with $\mathcal{H}$ constant) can be useful. Let us suppose that there is a statistically stationary regime $\overline{S}$, $\overline{T}$, $\overline{\mathcal{H}}$ (corresponding to chrons; we will see that such is indeed the case). In order to have a nontrivial solution, we must have

$$\overline{\mathcal{H}} = \frac{K_S K_T}{\omega^2}$$

($\overline{\mathcal{H}} > 0$; recall that K_T, $K_S > 0$), and then

$$\overline{S} = \frac{\overline{\mathcal{H}}\,\overline{T}}{K_s}, \quad \overline{S}\,\overline{T} > 0.$$

Indeed, this is approximately what we observe during the chrons of the model for the average values of $\mathcal{H}$, S, T (see section 3 and Figure 4). Now, suppose our dynamo model leaves this stationary state (chron state) to enter into a reversal or an excursion. According to the signs of $\overline{S}\,\overline{T}$, $\mathcal{H}$ must be negative for a certain period to make S decrease (this statement will be further clarified in section 3.2.2). During a reversal $\mathcal{H}$ varies significantly and its fluctuations are large compared with averaged values. We have no more $\overline{\mathcal{H}T} \approx \overline{H}\,\overline{T}$, and the behavior of the system is essentially determined by the way the different levels of cells are populated (see section 3.2.1).

2.2. Model of Turbulence

[11] A complete description of the model of turbulence without the retroaction of the magnetic field is given by *Blanter et al.* [1999]. It is a dynamic, time-dependent stochastic process, which may be described as a cellular automaton with long-range interaction.

[12] A conventional cellular automaton consists of a lattice of individual elements, each of which can be assigned a scalar property [*Wolfram*, 1986]. This scalar property will change as the result of (a) external forcing affecting all of the elements and (b) internal interactions between elements. External forcing is often assumed to occur at a constant rate, and the internal interactions are usually simplified to include only nearest neighbor interactions. The dynamo model to be presented here retains the simplicity of such conventional cellular automatons but differs in several important respects in order to represent a dynamo mechanism. First, an approximation of the magnetohydrodynamics interactions (see section 2.2) is used at all length scales, not only the smallest. This is because the structural properties of both the flow and the magnetic field may depend strongly on long-range interactions through differential rotation and turbulent motions. A second important assumption of the model is that, rather than being a simple scalar field, local helicity is quantified as a binary state, either strong or weak. In this way we can specifically account for the feedback process of the magnetic field on the helical motions.

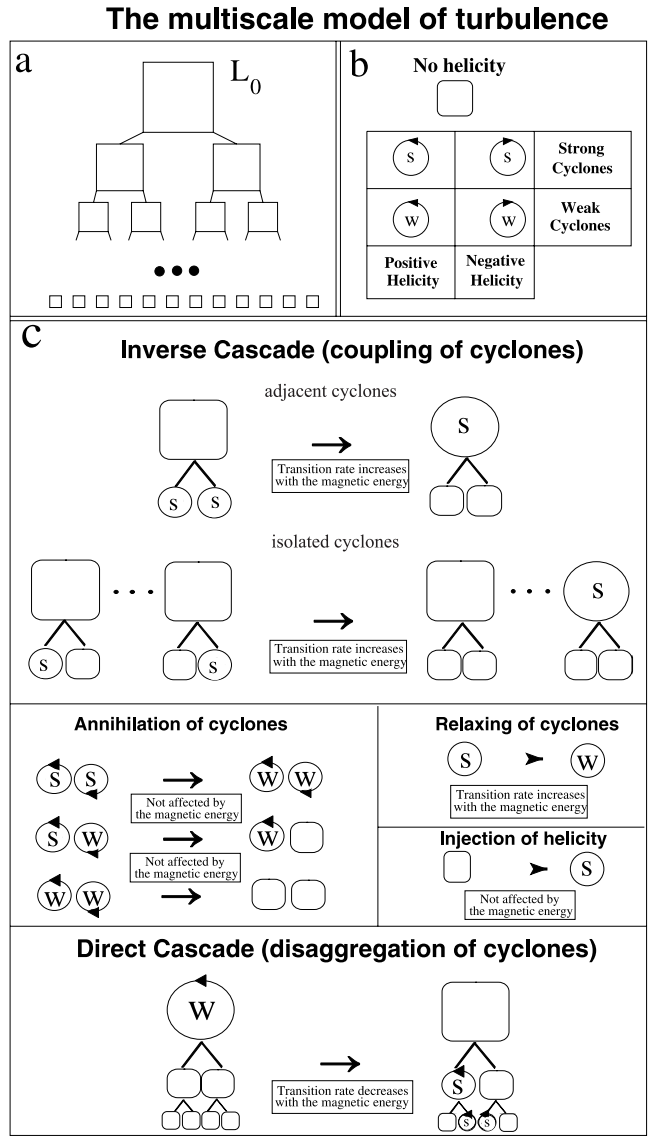

Figure 1. (a) Model of turbulence for the hierarchical structure of scales. (b) Five possible states. Helicity is positive, negative, or null; helical motions are quantified, strong or weak. (c) Transitions from one state to another in the model of turbulence based on next-neighbor interactions and long-range interactions (cascades). Insets indicate how the different transition rates are affected by the intensity of the magnetic fields.

[13] The model is rather abstract. It is assumed that cyclones of different length scales appear in hierarchically organized cells (Figure 1a). Each cell at level $(l + 1)$ is linked to a group of n cells at the previous level l. The length scale of a cyclone of level $l \leq L$ is $L_0 n^{l-L}$, L_0 being the characteristic length scale of the whole volume where the dynamo mechanism takes place. The number of cells at level l should vary as $n^{-3(l-L)}$ in order that the cyclones of each level l fill the space (like the largest level one). Here,

we simply take n^{l-L} (Figure 1a); indeed the properties of the model are not significantly changed by this simplification. Furthermore, again for the sake of simplicity, we take $n = 2$ (a common choice in this kind of model). If two cyclones of level l occupy a group of two cells linked to a cell of the upper level ($l + 1$), they are referred to as adjacent (otherwise, they are referred to as isolated) (Figure 1c). The model is a simplified representation of 3-D cyclonic structures (e.g., cyclones can be adjacent along the x, y, or z direction, without specification, x, y, z being three orthogonal directions). Furthermore, we will focus on the statistic evolution of the states of cells, as will be defined below (see equation (6)). In other words, we will not consider individual cell coordinates, but rather treat them as a whole. We will call this model a multiscale model.

[14] Cells of different dimensions at each scale level are assigned a state, which locally represents the sign of the dominant helical motions at this scale. Thus a cell may have positive, negative, or no helicity. Positive and negative helicity are associated with right-handed and left-handed cyclones, respectively. Taking into account the quantification of helicity, we end up with five different states (Figure 1b). This is the smallest number required to account for the sign and intensity of helical motions. Overall, in the absence of magnetic field, this conceptual model of turbulence is symmetric with respect to change in sign of helicity, in the sense that generation and evolution equations, as well as the random number generator, are the same for both helical motions.

[15] Interactions between cyclones are governed by repulsion (attraction) of antiparallel (parallel) electrical currents generated by these cyclones in the magnetic fields. Cyclones may form from the decomposition of larger ones or from the merging of smaller ones (Figure 1c) and the multiscale dynamics includes (1) a continuous transfer of helicity from larger to smaller scales (i.e., a direct cascade; disintegration of cyclones contributes to the appearance of cyclones at smaller scales), (2) a continuous transfer of helicity from smaller to larger scales (i.e., inverse cascade; coupling of cyclones contribute to the appearance of cyclones at larger scales), and (3) a permanent injection of helicity (cyclones may appear). We assume that newborn cyclones resulting from these multiscale interactions have strong helicity. In addition, relaxation and dissipation processes are taken into account at each scale: helicity may jump from a strong to a weak state and cyclones may disappear (Figure 1c).

[16] A stochastic ingredient is incorporated into the model by assuming that the entire system follows a Poisson process. More specifically, the different transitions shown in Figure 1c are governed by transition rates, i.e., probabilities per unit of time of making a transition from one state to another. These transition rates evolve depending on the present configuration of cyclones at all scales and the intensity of the magnetic field (section 2.3). Practically, they are determined from a set of constitutive equations which allow for incorporation of characteristic timescales for the physical processes being considered. For example, at the smallest length scale of the multiscale system, the elementary scale, the helical forcing is characterized by a constant rate E_0, the same for both orientations (i.e., mirror symmetry of the turbulence generation). In other words, with respect to this external forcing alone, the probability of an elementary cyclone appearing in an empty cell during an infinitesimal time interval dt is $E_0\,dt$; this also implies that the characteristic time during which an elementary cell remains empty is proportional to $1/E_0$.

[17] In some $\alpha\omega$ or α^2 models, it is assumed a priori that turbulence is not mirror-symmetric and the expression of helicity is given. Here, as mentioned above, we assume mirror-symmetric turbulence generation and cyclone evolution that is ruled by the same model parameters for both helicities. Nevertheless, the stochastic ingredient implies that symmetry breaking occurs [*Blanter et al.*, 1999]: at a given time and a given level, the population of cyclones can be predominantly of one kind (positive or negative); we call such a population asymmetric (mean helicity is not zero). Furthermore, our mechanism is necessarily homogeneous in the whole volume of the dynamo.

[18] From the cyclone population at time t, we estimate mean helicity, $\mathcal{H}(t)$, which enters the source term of the poloidal field in equation (5). It is simply computed as a weighted average of the differences between the numbers of cyclones of positive and negative helicity at all scales. Strong cyclones are given more weight than weak ones (by a ratio of at least 10 to 1), and the contribution of larger cyclones is greater than the contribution of smaller ones, according to a scaling law. Therefore mean helicity is

$$\mathcal{H}(t) = \zeta \sum_{k=1}^{K} \sum_{i=1}^{2} \frac{\rho_i (P_i(k,t) - Q_i(k,t)) \chi^k}{N_k} \tag{6}$$

where K is the total number of scales in the hierarchical system, ζ and χ are positive constants, N_k is the total number of cells of scale k; P and Q are the numbers of cyclones of positive and negative helicity, respectively; the index i is for strong ($i = 1$) and weak ($i = 2$) states; and $0 < \rho_2 \ll \rho_1$.

2.3. Retroaction of the Magnetic Field

[19] We define the magnetic energy as

$$W = S^2 + T^2. \tag{7}$$

Two types of retroaction are taken into account. First, we assume that an increasing W favors the appearance of larger spatial scales in the flow. This assumption is derived from the results of laboratory and numerical experiments on magnetic helical turbulence [*Frisch et al.*, 1975; *Pouquet and Patterson*, 1978] and laboratory experiments on the effect of large-scale magnetic fields on rotating fluid motions [*Brito et al.*, 1995], as well as from geomagnetic observations showing the persistence of large-scale magnetic fields and configurations of the core flow at the core-mantle boundary (CMB) [e.g., *Le Huy et al.*, 2000]. We implement the assumption for increasing W by reducing the transition rates for the direct cascade and by increasing those for the inverse cascade. This enhances the lifetime of weak, large-scale cyclones.

[20] Second, the transition rate from the strong state of a cyclone to the weak state is assumed to be proportional to W. This mimics the effect of the Lorentz force, since strong cyclones are much more efficient in producing helicity and hence magnetic fields, see equation (6). As a result, the

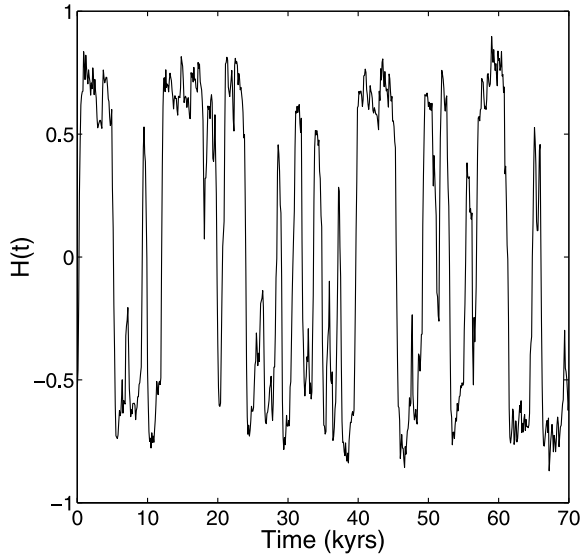

Figure 2. Change in normalized mean helicity $\mathcal{H}$ versus time (equation (6)). The sign of mean helicity shifts suddenly from positive to negative in no apparent order.

characteristic lifetime of strong cyclones rapidly decreases as magnetic field strength increases.

3. Results

[21] We now examine the temporal properties of the magnetic fields produced by the model as a function of the magnitude of helical forcing E_0. In this paper, $10^{-7} \leq E_0 \leq 10^{-2}$ and all other parameters of the model are kept constant. Taking $K_S^{-1} = 10^4$ years, we end up with a physical time unit of 1 year, which defines the maximum numerical time step. Let us first characterize some temporal properties of the flow without magnetic field.

3.1. Spontaneous Reorientation of Large-Scale Circulation

[22] When the model of turbulence operates in the absence of a magnetic field, it produces rapid fluctuations in the sign of mean helicity (Figure 2). In fact, helical motions at all scales, including the largest ones, abruptly change orientation [*Blanter et al.*, 1999]. These rapid fire changes in mean helicity indicate a spontaneous reorientation of large-scale circulation.

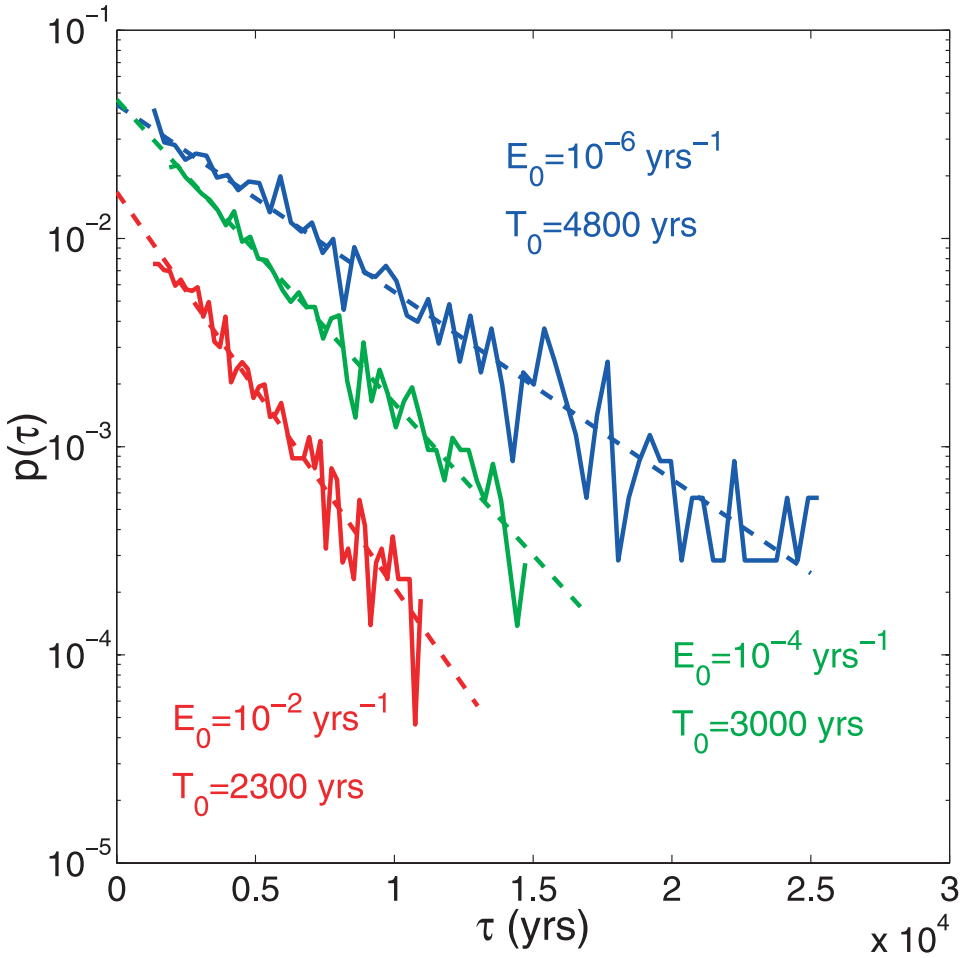

Figure 3. Probability density of the time duration between two sign changes of mean helicity for different E_0 values in the model implemented without magnetic fields. Dashed straight lines represent an exponential decay with a characteristic time T_0.

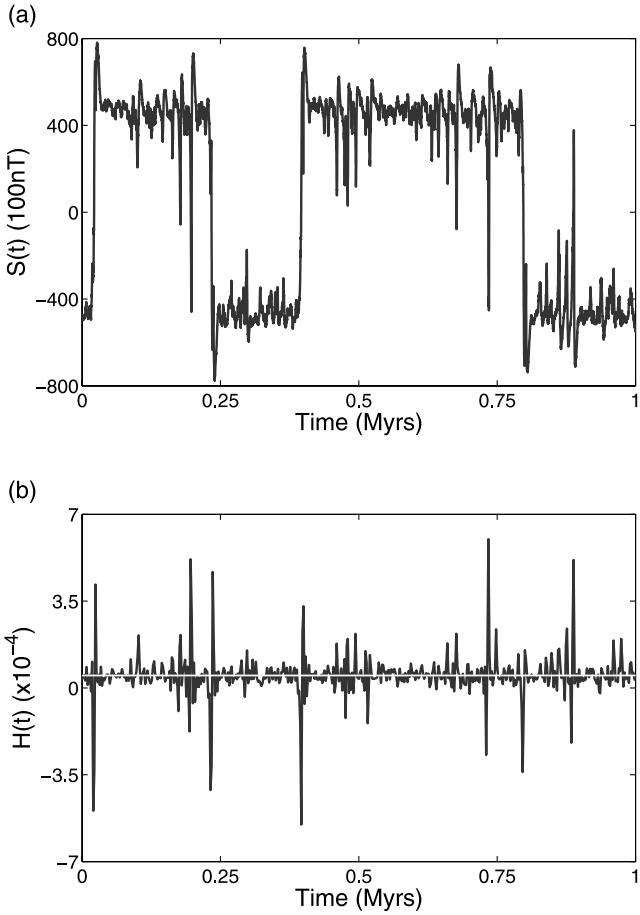

Figure 4. Evolution of (a) the poloidal field and (b) the mean helicity over 10^6 years for $E_0 = 4 \times 10^{-4}$ yr^{-1}. In Figure 4b the horizontal line indicates the value of $K_S K_T/\omega$.

[23] This behavior may be related to recent experiments in thermal convection at high Rayleigh number showing oscillatory large-scale circulation and reversals of the so-called mean wind [*Niemela et al.*, 2000]: the flow can organize itself at large scale, but changes sign frequently for high Rayleigh numbers (i.e. $Ra > 10^{11}$). Velocity statistics show that large-scale circulation is characterized by a distribution of the time intervals τ between two helicity reversals with an exponential tail [*Sreenivasan et al.*, 2002].

[24] Figure 3 shows that our model provides a similar distribution of τ when implemented without a magnetic field. The corresponding probability density function is

$$p(\tau) \sim \exp\left(-\frac{\tau}{T_0}\right), \tag{8}$$

where T_0 is a characteristic time. T_0 may be considered as an upper value of the time constants of large-scale circulation, or as a rough estimate of the correlation time for large-scale flow in the absence of a magnetic field.

[25] When magnetic field intensity is weak, the sign and amplitude of the α effect is likely to change over a short timescale not exceeding the characteristic time T_0 of the exponential decay law of formula (8). T_0 decreases when the forcing rate increases, but is always shorter than 5000 years for $E_0 > 10^{-7}$ yr^{-1}. T_0 is therefore shorter than the diffusive time $K_S^{-1} = 10^4$ years in the entire range of E_0 value studied in the paper. As shown in section 3.2.3, the sudden switches of mean helicity and the value of the time interval between two spontaneous reorientations of large-scale circulation are key in determining the duration of magnetic field reversals. T_0 depends on the parameters of the cascades, as discussed by *Blanter et al.* [1999], and also depends on E_0 as shown in Figure 3.

3.2. Reversal Sequences and Transient Regimes of Evolution

[26] In this section, we analyze the temporal evolution of the magnetic field with respect to statistical properties of the model of turbulence. Typical system behavior is presented in Figure 4a. We recognize periods of stable polarity, quick reversals, excursions, and secular variation. In order to identify the regimes generating such temporal behavior, we isolate two states associated with different magnetic field intensities: the reversal state characterized by low fields and the chron state characterized by high fields.

3.2.1. Reversal State

[27] When the model operates with magnetic fields, the conditions prevailing during different reversals are never the same, so a description of the reversal state is much easier when taking a simplified set of initial

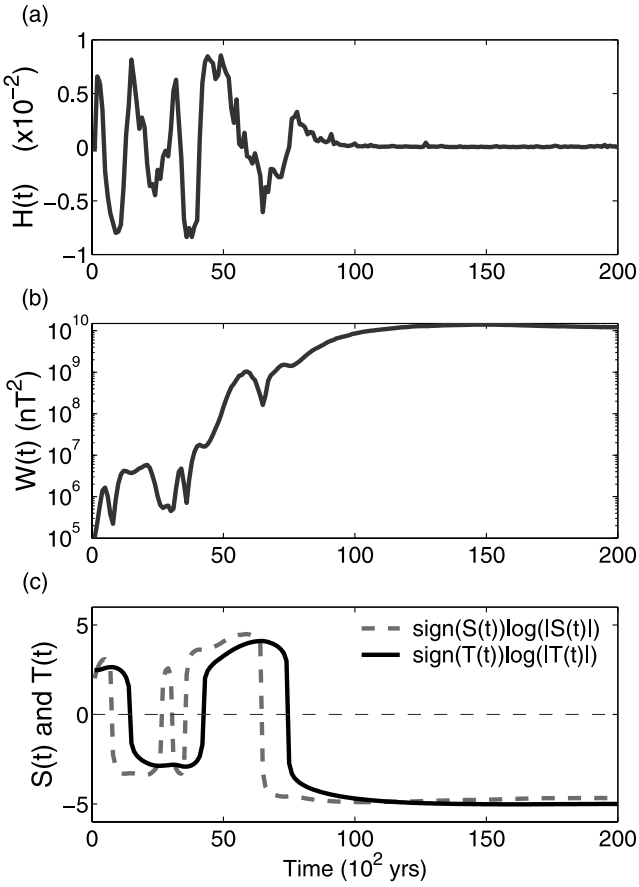

Figure 5. Changes in (a) normalized mean helicity, (b) magnetic energy W, and (c) the poloidal and toroidal fields over 2×10^4 years. Initial conditions are $\mathcal{H}(0) = 0$, $T(0) = 10 \times S(0) = 10$ nT, and $E_0 = 10^{-4}$ yr^{-1}.

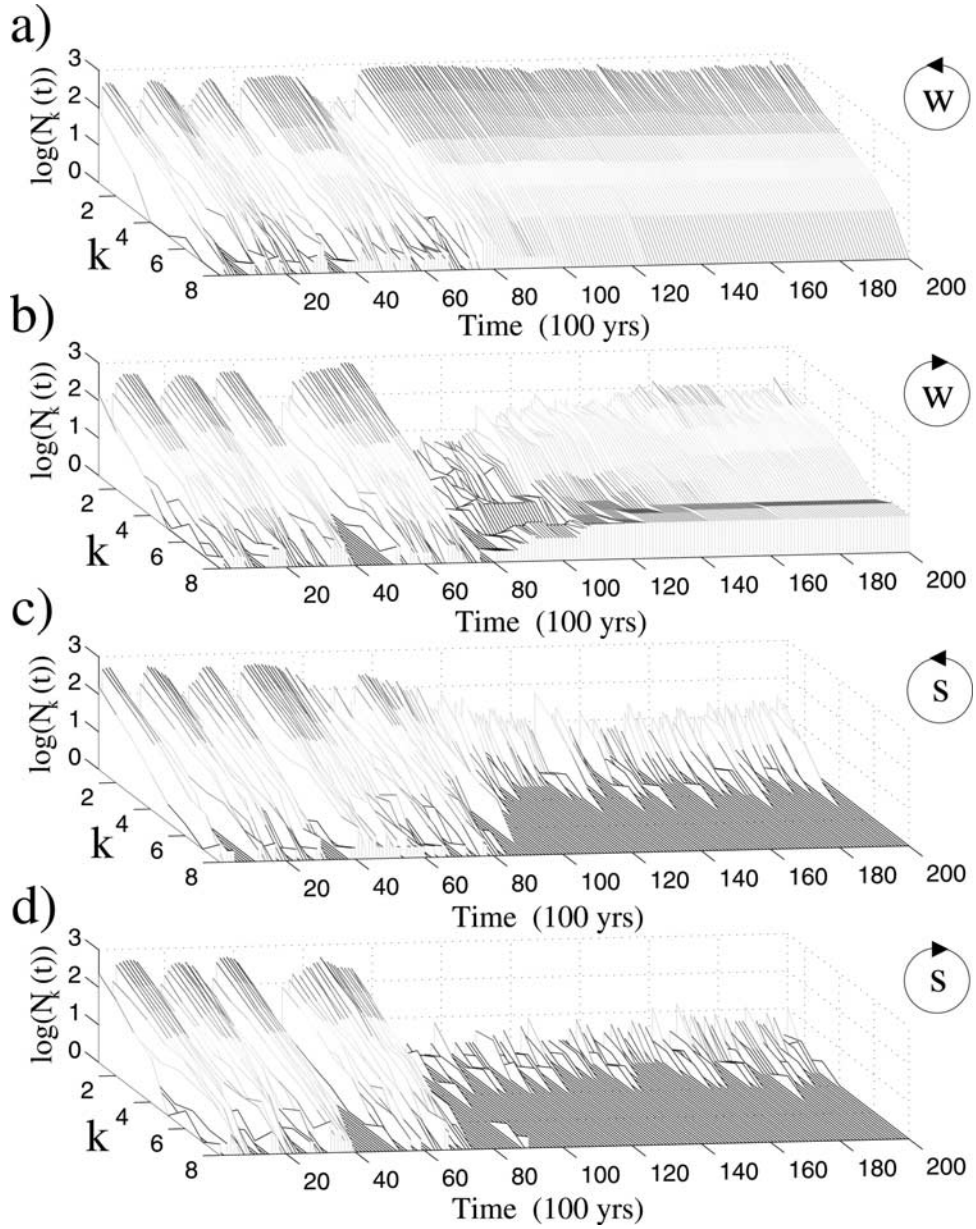

Figure 6. Evolution of cyclone populations over 2×10^4 years: (a) weak positive cyclones, (b) weak negative cyclones, (c) strong positive cyclones, and (d) strong negative cyclones. The mean helicity presented in Figure 5a may be inferred from these different cyclone populations. Note the evolution of the different populations with respect to the magnitude of magnetic energy (Figure 5b).

conditions: zero mean helicity (i.e., helical motions of both signs equally present) and magnetic fields with intensities 3 orders of magnitude lower than their mean values during the chrons. Figures 5a, 5b, and 5c show the change in magnetic energy of mean helicity, $S(t)$, and $T(t)$, respectively, over 2×10^4 years starting from such initial conditions. For the same period of time, Figure 6 shows the evolution of the different cyclone populations.

[28] As mentioned in section 3.1, weak magnetic fields allow for rapid fluctuations in mean helicity (Figure 5a). The amplitude of these fluctuations puts the system into a supercritical state (in which its evolution is further accelerated) if positive cyclones dominate the flow ($\mathcal{H}(t) > 0$). Hence the model of turbulence is extremely efficient in amplifying a weak, preexisting magnetic field because the fields can evolve more rapidly when they diffuse over timescales shorter than T_0. For example, the poloidal field rapidly increases in intensity from an incipient toroidal field when $\mathcal{H}(t)$ becomes positive. Then the intensity of both magnetic fields increases rapidly because of positive feedback between equations (4) and (5), mimicking runaway growth in magnetic field intensity.

[29] This exponential growth in magnetic field intensity is limited by a combination of effects as the flow configuration increases the amount of magnetic energy (Figure 5b). First, strong magnetic fields amplify the inverse cascade. As a consequence of the asymmetric state at small scales when

$\mathcal{H}(t) > 0$, positive helical motions (Figures 6a and 6c) rapidly dominate the flow at increasingly larger scales. Second, strong magnetic fields rapidly decrease the lifespan of strong vortices. Thus magnetic field intensity stops growing because the flow becomes composed essentially of positive but weak vortices (Figure 6a). Third, strong magnetic fields impede direct cascade. This increases the lifespan of weak vortices, stabilizing the flow at larger scales and therefore preventing new (strong) large-scale cyclonic motions from occurring. As a result, increases in magnetic field strength promote weak vortices to the detriment of strong ones (compare Figures 6a and 6b with Figures 6c and 6d) and strengthen the predominance of positive helical motions (compare Figures 6a and 6c with Figures 6b and 6d). Finally, the magnetic fields reach equilibrium values around which they start to fluctuate (section 2.1). This corresponds to the initiation of a chron, i.e., a period of time much longer than K_S^{-1} during which the magnetic field does not change signs.

[30] In conclusion, from weak magnetic fields and a purely symmetric state of flow (i.e., zero mean helicity), an amplification mechanism generates strong fields, which will last for long periods of stable polarity during which circulation is characterized by the predominance of positive helical motions (strong or weak). Figure 5 allows us to follow the way fields are generated step by step; the details of this process are not predictable due to the highly complex behavior of $\mathcal{H}$. Note that during true reversals (between two chrons), after a collapse of the poloidal component, the fields are regenerated quicker than in the present case; T indeed does not go to zero.

3.2.2. Chron State

[31] At the beginning of a chron, the magnetic fields produced by the model are extremely stable and small-scale helical motions are sufficient to compensate for diffusion. During this period, small fluctuations in field intensity are observed (Figure 4), corresponding to secular variation. Later, these fluctuations tend to increase. In addition to secular variation, excursions occur during which the intensity of the poloidal field becomes extremely low or the field even changes sign for a short period of time (Figure 4). Finally, polarity reversals may occur (Figure 4). Despite a strong stochastic ingredient, these polarity switches do not occur only by chance; they are the result of the long-term evolution of cyclone populations.

[32] Dissipation is more active at smaller scales where magnetic diffusion is more efficient (section 2.3). To compensate for dissipation, new helical motions are more likely to occur at smaller scales, and external forcing in the presence of large scale magnetic fields may be described as the result of the input of microscopic helical flow. On the other hand, the characteristic timescale of large-scale circulation is controlled by the intensity of the magnetic field. The largest-scale structures cannot disappear if the magnetic field is strong (section 2.3), and it is only when it weakens that changes in large-scale flow can occur. The only way to reduce the intensity of the magnetic field is to have a predominance of negative cyclones at some scales ($\mathcal{H}(t) \rightarrow 0$ in equation (5)) for a certain period. When field intensity is high, such population inversions are only possible at the smallest scales through the stochastic ingredient in the forcing mechanism. At the smallest scale, population inversions occur with a frequency which can be determined from the magnitude of the forcing E_0. When this happens, the intensity of the magnetic field decreases and cyclonic motions of negative helicity are therefore more likely to propagate to larger scales. Then, as one proceeds in the chron, the difference in populations between the two types of helical motions tends to disappear at increasingly larger scales. This long-term evolution is amplified by the concomitant fluctuations in magnetic field intensity.

[33] In conclusion, changes in stable polarity intervals are characterized by a progressive population inversion at all scales, from a predominance of positive cyclones due to the initiation of the chrons to a predominance of negative cyclones responsible for the collapse of the magnetic field leading to a reversal. The long-term evolution between reversals may be described as an emergent property of the model that arises spontaneously from multiscale dynamics. By emergent, we mean that one phenomenon leads to another, not in a direct cause/effect relationship, but in a manner that involves pattern of interactions between the elements of a system over time [*Andler et al.*, 2002].

3.2.3. Reversal Process

[34] The evolution of the different cyclone populations also provides an understanding of the reversal mechanism. Strong cyclones show complex evolutionary patterns resulting from long-range interactions associated with helicity transfer (i.e., cascades) and external forcing. Weak cyclones evolve locally at a rate depending on the intensity of the magnetic field. As a consequence, populations of weak cyclones provide a more stable estimate of the current state of the evolution toward the reversal. As shown in Figure 7, different regimes can be characterized by the mean helicity of weak cyclones averaged at all scales

$$\epsilon(t) = \frac{1}{K}\sum_{k=1}^{K} \frac{P_2(k,t) - Q_2(k,t)}{N_k}. \qquad (9)$$

[35] For different chrons, Figures 7b, 7d, and 7f show a similar logarithmic decay of ϵ with time before the end of the chron, in addition to the statistical fluctuations associated with the injection of turbulence. As rendered by the logarithmic trend, this inversion is accelerated further as negative cyclonic motions propagate to increasingly larger scales.

[36] Reversals become possible when the difference in population between the two types of cyclonic motions vanishes at all scales ($\epsilon = 0$ in Figures 7b, 7d, and 7f). Indeed, the symmetry of the system is restored and strong vortices of negative helicity can propagate to the largest scale of the system. Significantly high negative values for mean helicity are then likely to be observed (see the ϵ value close to the reversals in Figure 7). Thus the poloidal magnetic field produced by the α effect changes sign and the intensity of this field collapses. Field strength becomes very low and no longer affects the circulation of the fluid. Then, as explained in section 3.2.1, over the characteristic time T_0, helical motions allowing the runaway growth of the magnetic fields are likely to occur. From a predominance of negative to a predominance of positive helical motions, spontaneous reorientations of large-scale circulation strongly affect the populations of weak cyclones as shown in Figures 7c, 7e, and 7g by the abrupt change of sign for

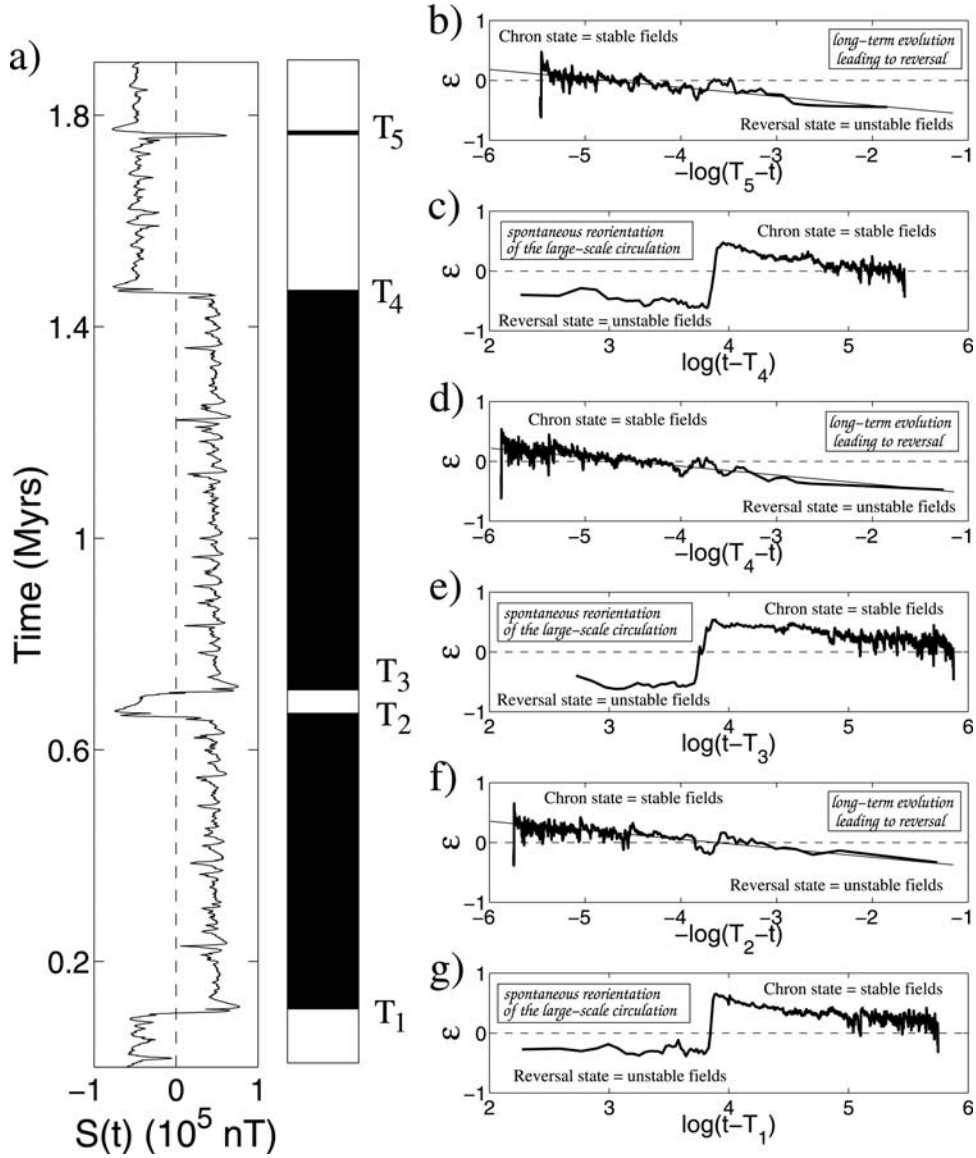

Figure 7. (a) Evolution of the poloidal magnetic field and the corresponding polarity timescale over 1.9×10^6 years for $E_0 = 10^{-4}$ yr^{-1}. (b)–(g) Evolution of ϵ over three different chrons, i.e., [T_4; T_5], [T_3; T_4], and [T_1; T_2]. We use different logarithmic timescales to emphasize two transient regimes of evolution over short and long periods: (1) over short periods, spontaneous reorientation of large-scale circulation at the beginning of the chrons (Figures 7g, 7e, and 7c) and (2) over long periods, long-term evolution leading to reversals (Figures 7f, 7d, and 7b). A straight line, always with the same slope, indicates a logarithmic decay with respect to the time before the end of the chron.

ϵ (over relatively short periods compared with the time elapsed since the beginning of the chron). This marks the end of the reversal mechanism, which may also lead to an excursion if the magnetic field maintains the same polarity as before.

[37] Figure 8 shows the evolution of the poloidal magnetic field over short time periods before and after different reversals. In the vast majority of studied cases, magnetic field intensity is lower before the reversal than after, and reversal duration is in the order of T_0, the upper time constant for large-scale circulation without a magnetic field (section 3.1). The relationship between reversal duration and T_0 may be explained as follows.

[38] The origin of a reversal is, as described earlier, a negative α effect resulting from the predominance of negative cyclonic motions. As a consequence, the poloidal magnetic field reverses before the toroidal field, and lower values for magnetic energy imply that positive helical motions are likely to dominate flow again after a time period shorter than T_0 (section 3.1). T_0 being shorter than the diffusive time of large-scale magnetic fields, magnetic field strength is still high when the flow changes orientation, and a positive α effect allows magnetic fields, and in particular the poloidal field, to rapidly reach their equilibrium values. As a result, T_0 is a good estimate of reversal duration because with the exception of the time required

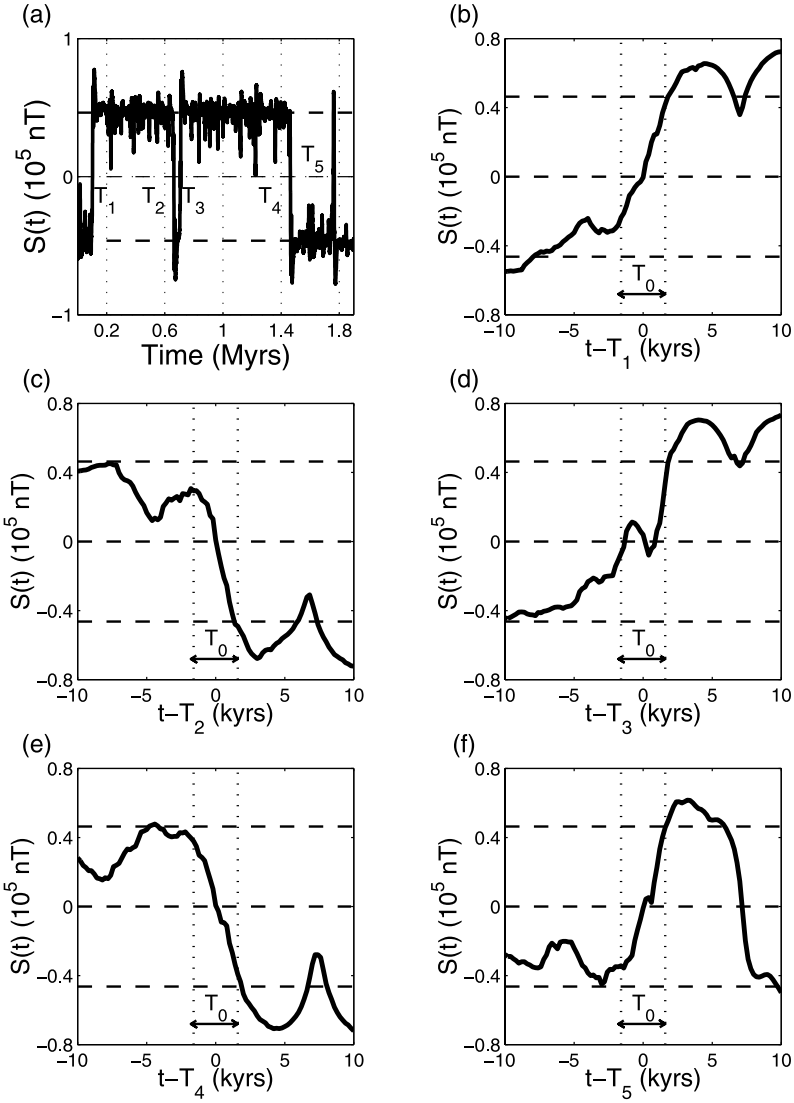

Figure 8. (a) Evolution of the poloidal magnetic field over 1.9×10^6 years for $E_0 = 10^{-4}$ yr^{-1} (see Figure 7). (b)–(f) Zoom of different time intervals of 2×10^4 years, with time measured from different reversal times $T_{\{1,2,3,4,5\}}$. The dashed lines indicate zero as well as positive and negative mean values for the poloidal magnetic field over long periods. The time interval between the dotted lines is $T_0 = 3 \times 10^3$ years (see Figure 3).

for spontaneous reorientation of large-scale circulation, the poloidal magnetic field evolves very rapidly from and toward its equilibrium values.

3.3. Reversal Rate and Excursions

3.3.1. Reversal Rate

[39] Figure 9 shows the cumulative distributions of chron durations for three different values of E_0, and the best fitting exponential curve $\exp(-t/T_{\text{mean}})$. This reasonable fit shows that the model distribution concords with geodata [*Merrill et al.*, 1996] and that reversals occur randomly with respect to a characteristic time T_{mean} that decreases as the E_0 value increases.

[40] The frequency of population inversions at small length scale increases with the magnitude of the stochastic injection of turbulence E_0, producing larger variations in the magnetic fields and accelerating the long-term evolution leading to reversals. Figure 10 shows the evolution of the poloidal magnetic field over 60 Myr for three different values of the external forcing rate E_0. Reversals, excursions, and secular variation are omnipresent features; the reversal rate and the energy of the secular variation increase when the E_0 value increases.

[41] This relationship between the external forcing rate E_0 and the duration of the chron links the microscopic structure of the flow and large-scale magnetic field behavior. It can be analyzed systematically through numerical modeling, as illustrated by Figure 11. In Figure 11, we only consider chrons longer than 10^4 years. In cases of over 4 orders of magnitude, a straight line indicates a power law relationship

$$\Delta \sim E_0^{-a} \tag{10}$$

with $a = 0.43$ and Δ the mean chron duration. The reversal rate changes by an order of magnitude when the

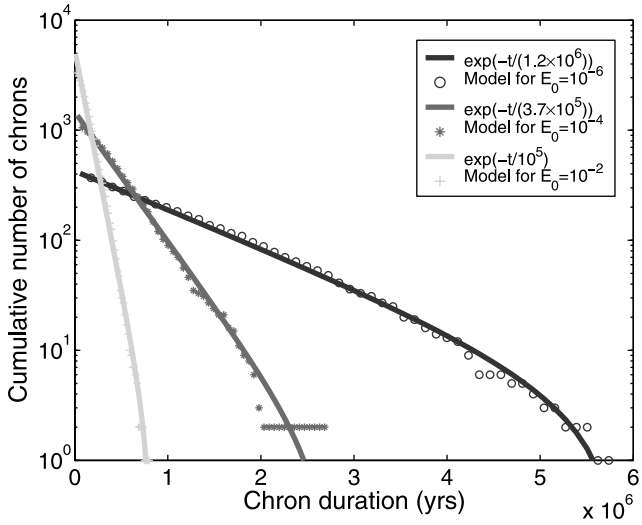

Figure 9. Comparisons between cumulative distributions of chron durations of the model and an exponential law $\exp(-t/T_{\text{mean}})$.

characteristic time scale of the microscopic helical flow changes by 2 orders of magnitude.

[42] Below $E_0 \approx 3 \times 10^{-7}$, the dynamo mechanism is unable to either generate or maintain large-scale magnetic fields. In fact, the injection being too weak, dissipation dominates at small scale, and helical motions cannot propagate to higher scales. This limit indicates the conditions required for our dynamo mechanism to work. Figure 11 also shows that reversals occur at all E_0 values, from the limit of dynamo action ($E_0 \approx 3 \times 10^{-7}$) to the limit at which periods of stable polarity can no longer be identified between reversals ($E_0 \approx 10^{-2}$).

3.3.2. Excursion Rate

[43] It is possible to analyze the temporal distribution of excursions over different chrons of different durations. The temporal evolution of magnetic fields could be expected to yield some precursory patterns as flow slowly evolves toward a reversal phase. However, Figure 12 shows that the excursion rate is constant. This result indicates that despite the continuous evolution of flow patterns during a chron, excursions are more a reflection of the constant injection rate of helicity than the acceleration process toward a reversal.

4. Discussion

[44] Periods of stable polarity, excursions and reversals appear to be systematic temporal patterns of the magnetic fields generated by our model. None of these features is imposed: they result from the feedback process between large-scale magnetic fields and turbulence and explicitly take into account statistical fluctuations, scaling and interaction terms. Thus the fluctuations of the dipole field as well as the transient regimes of evolution responsible for the initiation of chrons or the onset of reversals are intrinsic properties of our system.

4.1. Main Features of the Model

[45] The multiscale dynamo model is a dissipative system (dissipation essentially takes place at small scales) in which the permanent transfer of mechanical to magnetic energy

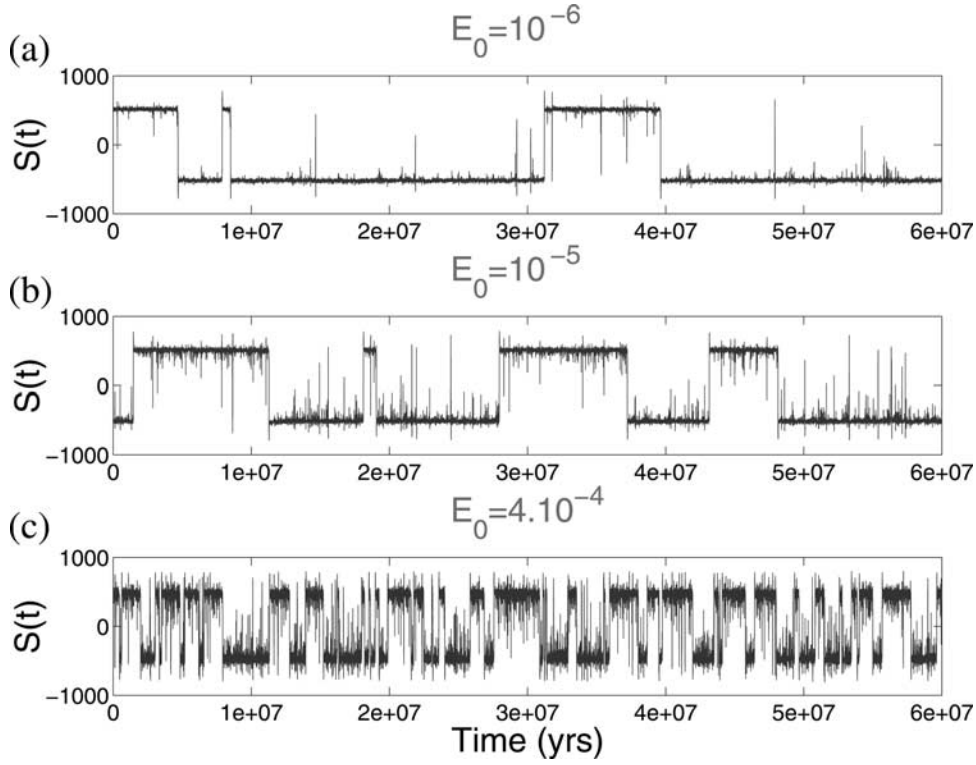

Figure 10. Evolution of the poloidal magnetic field over 60 Myr for three different values of the external forcing rate: (a) $E_0 = 10^{-6}$ yr^{-1}, (b) $E_0 = 10^{-5}$ yr^{-1}, and (c) $E_0 = 4 \times 10^{-4}$ yr^{-1}.

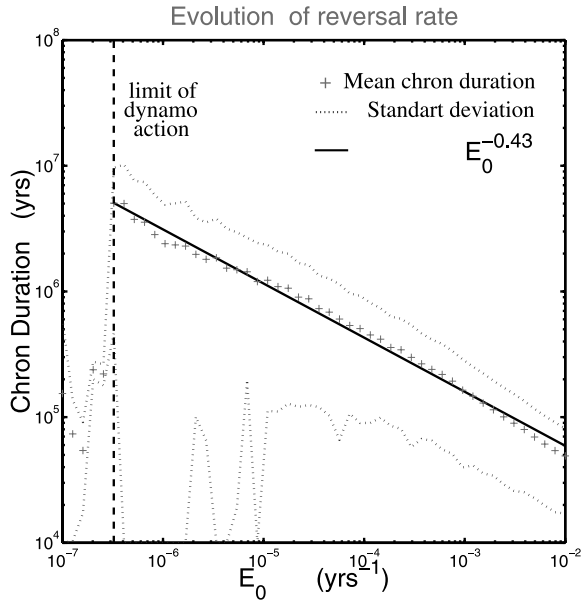

Figure 11. Evolution of the mean chron duration versus the external forcing rate E_0. Note the logarithmic scale for both axes. The dotted lines correspond to the standard deviation for the duration of a single chron; the solid line illustrates a power law decay with exponent $a = -0.43$; the dashed line marks the E_0 value below which the dynamo mechanism is unable to generate and maintain large-scale magnetic fields.

and vice versa occurs in such a way that energy conservation can be ensured (e.g., Figure 5).

[46] Classical $\alpha\omega$ dynamo are based notably on the hypothesis that small-scale cyclonic motions are able to generate large-scale magnetic fields through the so-called α effect [*Krause and Rädler*, 1980]. Here, we use a multiscale α effect and assume that helical motions at all scales are able to interact with preexisting magnetic fields. Our saturation mechanism has an impact on the α effect similar to the simpler quadratic quenching considered by *Hoyng et al.* [2001]. However, in our model, quenching is a consequence of the feedback mechanism of magnetic fields on fluid dynamics, a feedback that is responsible for a wide variety of behaviors (e.g., emergence of population inversion, reversals of short duration).

[47] Symmetry considerations help us understand periods of stable polarity, reversals, excursions, and secular variation in a general process of evolution. A break in symmetry marks the end of a reversal, triggering the reactivation of dynamo action. Later, during chrons, strong magnetic fields imprint the memory of the last reversal on the flow by sustaining this asymmetric state. The injection of turbulence at small scales slowly erases this memory and leads to a reversal. Small-scale dynamics therefore play an essential role in gradually destroying the stable interaction between flow and magnetic fields at large scales. In fact, helical forcing slowly and progressively changes the population of cyclones at all scales and reinforces the symmetry of the system. A reversal may then be triggered as the magnetic fields collapse. Spontaneous reorientations of large-scale circulation are then likely to occur, which reactivate the dynamo action. Thus we obtain a succession of stable polarity intervals with strong magnetic fields. Secular variation and excursions accompany the long-term evolution toward reversals.

4.1.1. Reversal Duration

[48] In our numerical experiments, underlying turbulence produces sudden fluctuations in mean helicity. There is a characteristic time during which the helical motions responsible for the collapse of magnetic fields are likely to be replaced by opposite helical motions that amplify magnetic fields. The system takes advantage of the collapse of the magnetic field to recover its dynamo efficiency (the system is resilient). Average reversal duration is then given as the higher time constant of the abrupt sign changes in mean helicity. There is a relationship of negative dependence between reversal duration and the magnitude of external helical forcing (Figure 3). Future polarity is determined during reversals by both the sign and intensity of the magnetic fields at the time when mean helicity suddenly changes sign. Extended to the geodynamo, these results predict reversals shorter than 5×10^3 years over the entire range of helical forcing in which there is dynamo action. They also predict longer reversals when the reversal rate is lower (through E_0), as well as a reversal process without memory.

4.1.2. Chron Duration

[49] The amplitude of helical forcing determines the mean chron duration through an evolution process that increases the correlation length of cyclonic activity. In many domains of physics, the concept of correlation length is crucial to estimating a system's sensitivity to perturbations. On the basis of the reversal mechanism described in this paper, we suggest that the correlation length of the flow may be an accurate estimate of the resistance of a chron. Indeed, on

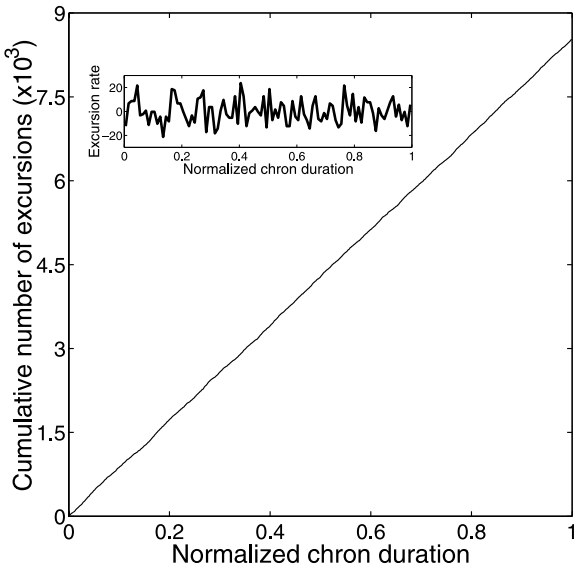

Figure 12. Temporal distribution of excursions. The time of the excursion from the last reversal ($T_{ex} - T_{i-1}$) is normalized by chron duration $T_i - T_{i-1}$. The linear trend indicates that excursions occur at a constant rate. The onset indicates the excursion rate when the linear trend is removed.

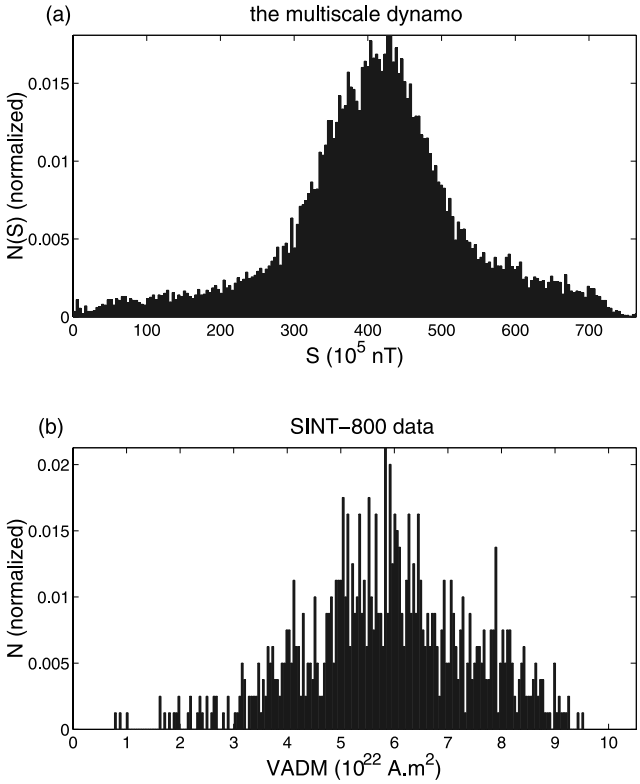

Figure 13. (a) Distribution of the intensity of the poloidal field of the model for $E_0 = 6 \times 10^{-4}$ yr^{-1}. (b) Distribution of the VADM of the Earth's dipole field obtained by *Guyodo and Valet* [1999].

one hand, at the initiation of a chron, the system stabilizes large-scale helical motions that limit both the injection of turbulence and the propagation of helical instabilities at smaller scales, preventing reversals from occurring. On the other hand, the stochastic ingredient in the helical forcing ($\sim E_0$) increases the correlation length of cyclonic activity by restoring the symmetry of the system at increasingly larger scales. During this phase, except at the very beginning of the chron, secular variation and excursions occur at a constant rate, for a given permanent helical forcing. Eventually, reversals may be triggered when the correlation length becomes infinite, i.e., comparable to the system size.

[50] The relationship between reversal rates and the magnitude of helical forcing (Figure 11) suggests that, during chrons, population inversion is always at work, no matter what the magnitude of E_0. The observed logarithmic decay of the mean helicity of weak cyclones indicates that chrons are actually readjustment periods between reversals. The characteristic time scale of this readjustment process may be given by the average duration of a chron.

[51] The erosion of system resistance during chrons implies that reversals always occur; superchrons do not constitute a specific regime of our dynamo. Instead, an ordinary reversal regime may by chance generate a superchron (extreme event) if helical forcing becomes extremely low. The real data analysis presented by *Jonkers* [2003], which also suggests that the geodynamo operates as a self-organized complex system, supports this hypothesis.

4.2. Application to the Earth

[52] The implication for the Earth's (mean) dipole field would be that reversals do not occur without warning, but only after the gradual formation of cyclonic structures of increasing dimension, providing a natural explanation of the saw-tooth patterns often observed in paleomagnetic data on geomagnetic fields [*Valet and Meynadier*, 1993]. On the other hand, there would be no systematic precursory behavior in dipole field fluctuations, since secular variation and excursions occur at a constant rate. The frequency of excursions in model simulations dovetails with paleomagnetic data [*Guyodo and Valet*, 1999], but the limited number of excursions documented to date makes a quantitative comparison premature.

[53] As for the secular variation, *Hoyng et al.* [2002] have shown that stochastic helicity fluctuations in an $\alpha\omega$ mean field models can reproduce the observed variability in geomagnetic dipole intensity during the Brunhes polarity chron. This is more or less the case here as well, as shown by comparisons between the statistical distribution of the virtual axial dipole moment (VADM) of the geomagnetic field over the past 8×10^5 years and the distribution of the intensity of our synthetic poloidal field for $E_0 = 6 \times 10^{-4}$ yr^{-1} (Figure 13). This value of helical forcing yields a mean chron duration of 2×10^5 years (Figure 11) and a mean reversal duration of 2.7×10^3 years (equation (8)).

[54] We are therefore able to reproduce, in a unified framework, the major observational constraints on the Earth's dipole evolution over the last 10^7 years (i.e., secular changes, reversal duration, chron duration). The analysis can be repeated for a lower reversal rate of 10^{-6} yr^{-1}, similar to the reversal rate observed 6×10^7 years ago at the end of the Cretaceous superchron. In this case, the model predicts a reversal duration of 4×10^3 years and a smaller variance of the secular variation (unfortunately more difficult to check).

[55] Helicity input depends on buoyancy input. Buoyancy is provided to the core flow by release of lighter material at the inner core boundary (ICB), both warmer and richer in light elements, as the solid inner core cools and increases in size by freezing. Because of Earth's rotation and high Reynolds number, this buoyant flow is helical turbulent, and it may be that helicity is injected at small scales [*Moffatt and Loper*, 1994]. In our model, the magnitude of helical forcing (E_0) must vary over more than one order of magnitude to explain the increase in the reversal rate since the cretaceous superchron. It is safe to assume that such a variation in the reversal rate requires a variation in the convection regime in the outer core. This evolution has to be faster than the average slow variation resulting from cooling of the core under constant conditions at the CMB (computed by averaging over the mantle time constant [*Labrosse et al.*, 1997]). On timescales of 10^7–10^8 years, changes in mantle convection due to geodynamical events could be invoked. For example, heat flux at the CMB may be sensitive to the geometry of the subduction zones [*Labrosse*, 2002], with heat transfer across the mantle decreasing with the characteristic length of the convection cells. It could be expected that heat flux at the CMB has

increased over the last 8×10^7 years because of the opening of the Atlantic. Should this prove to be the case, higher dissipation in the outer core would result, as well as changes in helicity input, since the effect of buoyancy forces balances dissipation. Of course, these considerations remain highly speculative but may deserve further research.

[56] One prediction the model makes is that worldwide geomagnetic events are more likely to occur when a reversal is near (i.e., when the correlation length of helicity fluctuation is increasing). These events could include excursions, large secular variation events, which could be searched for in paleomagnetic databases, and geomagnetic jerks, which are detectable from observatory and satellite data [e.g., *Courtillot et al.*, 1978; *Macmillan*, 1996]. Note that observations of the historical and archeomagnetic fields suggest the field is presently in a state which could announce a reversal. The dipole has been weakening by 0.05% yr^{-1} for the last 2×10^3 years, and *Bloxham et al.* [1989] and *Hulot et al.* [2002] suggest that patches of reverse flux are growing. The surface expression of the flow (i.e., the flow computed at the CMB using present-day secular variation data [e.g., *Roberts and Scott*, 1965; *Gire and Le Mouël*, 1989]) shows vortices of different scales, from the smallest scale accessible from data collected at the Earth's surface to the largest possible one (half the core circumference). Prograde and retrograde vortices are approximately equal in occurrence [*Le Huy et al.*, 2000] (of course, helicity should also be considered). We could speculatively argue that this observation is also indicative of a flow configuration close to a critical point, i.e., the onset of a reversal.

5. Conclusions

[57] We used our model to determine the physical basis of the characteristic timescales of reversals and chrons. Rapid reversals result from spontaneous reorientation of large-scale circulation in the absence of strong fields, while small-scale turbulence exerts considerable influence over the systematic evolution of the system toward reversals during chrons. In relation to turbulent flow, the multiscale dynamo model predicts an increasing correlation length scale of cyclonic activity as a reversal is approached.

[58] The model does have significant limitations. Considering only statistical values over the volume of the dynamo excludes any localization; we took an initial step to remedy this situation in *Blanter et al.* [2002]. In its present state, the model makes it virtually impossible to take into account the influence of the solid conductive inner core. Helicity injection at small scale as well as the mechanism of cyclone interactions are treated in a formal way. Both could be put on more solid physical ground. However, our objective should not be to abandon the basic idea, which is to capture the main features of the dynamo mechanism through a number of general and abstract concepts. Our model complements more conventional approaches by analyzing generic behaviors for turbulent dynamo action. Its emerging temporal patterns, which explain a wide range of observations, and the mechanism of emergence itself, may not depend strongly on the chosen representation. We believe that some of the general dynamo mechanism features observed in our model, including the reorientation of large-scale flow during reversal and the trend of chrons toward reversal through a kind of erosion process of the flow organization, will be repeated in continuous and more detailed models, such as the numerical dynamos solving the complete MHD equations.

[59] **Acknowledgments.** The paper was improved by the constructive comments of David G. McMillan, Jeffrey J. Love, and an anonymous reviewer. The authors are grateful to Kathy Whaler for her work on a previous version of this paper and Yohan Guyodo for the SINT-800 data. At the University of Edinburgh, Clément Narteau was supported through a Marie Curie fellowship HPMFT-2000-00669 from the European Community.

References

Andler, D., A. Fagot-Largeault, and B. Saint-Sernin (2002), *Philosophie des Sciences*, Gallimard, Paris.

Bak, P. (1997), *How Nature works*, Oxford Univ. Press, New York.

Blanter, E. M., C. Narteau, M. G. Shnirman, and J.-L. Le Mouël (1999), Up and down cascade in a dynamo model: Spontaneous symmetry breaking, *Phys. Rev. E*, *59*, 5112–5123.

Blanter, E. M., M. G. Shnirman, and J.-L. Le Mouël (2002), Up and down cascades: Three-dimensional magnetic field model, *Phys. Rev. E*, *65*, (6 Pt 1):061105-06110515.

Bloxham, J., D. Gubbins, and A. Jackson (1989), Geomagnetic secular variation, *Philos. Trans. R. Soc. London*, *329*, 415–502.

Braginsky, S. I., and P. H. Roberts (1987), A model geodynamo, *Geophy. Astrophy. Fluid Dyn.*, *38*, 327–349.

Brito, D., P. Cardin, H.-C. Nataf, and G. Marolleau (1995), Experimental study of a geostrophic vortex of gallium in a transverse magnetic field, *Phys. Earth Planet. Inter.*, *91*, 77–98.

Bullard, E. C. (1955), The stability of a homopolar dynamo, *Proc. Cambridge Philos. Soc.*, *51*, 744–760.

Cande, S., and D. V. Kent (1995), Revised calibration of the geomagnetic polarity timescale for the Late Cretaceous and Cenozoic, *J. Geophys. Res.*, *100*, 6093–6095.

Courtillot, V., J. Ducruix, and J.-L. Le Mouël (1978), Sur une accélération récente de la variation séculaire du champ magnétique terreste, *C. R. Acad. Sci.*, *287*, 1095–1098.

Dormy, E., J. Valet, and V. Courtillot (2000), Numerical models of the geodynamo and observational constraints, *Geochem. Geophys. Geosyst.*, *1*, doi:10.1029/2000GC000062.

Frisch, U., J. Léorat, A. Mazure, and A. Pouquet (1975), Possibility of an inverse cascade in MHD helical turbulence, *Fluid Mech.*, *68*, 769–778.

Gailitis, A., O. Lielausis, S. Dement'ev, A. Cifersons, G. Gerbeth, T. Gundrun, F. Stefani, M. Christen, and G. Will (2000), Detection of a flow induced magnetic field eigenmode in the Riga dynamo facility, *Phys. Rev. Lett.*, *84*, 4365–4366.

Gire, C., and J.-L. Le Mouël (1989), Tangentially geostrophic flow at the core-mantle boundary compatible with the observed geomagnetic secular variation: The large-scale component of the flow, *Phys. Earth Planet. Inter.*, *59*, 259–287.

Glatzmaier, G. A., and P. H. Roberts (1995a), A three-dimensional convective dynamo solution with rotating and finitely conducting inner core and mantle, *Phys. Earth Planet. Inter.*, *91*, 63–75.

Glatzmaier, G. A., and P. H. Roberts (1995b), A three-dimensional self-consistent computer simulation of a geomagnetic field reversal, *Nature*, *377*, 203–209.

Guyodo, Y., and J.-P. Valet (1999), Global changes in intensity of the Earth's magnetic field during the past 800 kyr, *Nature*, *399*, 249–252.

Hide, R. (1995), Structural instability of the rikitake disk dynamo, *Geophys. Res. Lett.*, *22*, 1057–1059.

Hollerbach, R., C. E. Barenghi, and C. A. Jones (1992), Taylor's constraint in a spherical $\alpha\omega$ dynamo, *Geophys. Astrophy. Fluid Dyn.*, *67*, 1–25.

Hoyng, P., M. A. Ossendrijver, and D. Schmitt (2001), The geodynamo as a bistable oscillator, *Geophys. Astrophys. Fluid Dyn.*, *94*, 263–314.

Hoyng, P., D. Schmitt, and M. A. Ossendrijver (2002), A theoritical analysis of the observed variability of the geomagnetic dipole field, *Phys. Earth Planet. Inter.*, *130*, 143–157.

Hulot, G., C. Eymin, B. Langlais, M. Mandea, and N. Olsen (2002), Small-scale structure of the geodynamo inferred from Oersted and Magsat satellite data, *Nature*, *416*, 620–623.

Jault, D. (1995), Model Z by computation and the taylor's condition, *Geophys. Astrophy. Fluid Dyn.*, *79*, 99–124.

Jonkers, A. R. T. (2003), Long-range dependence in the Cenozoic reversal record, *Phys. Earth Planet. Inter.*, *135*, 253–266.

Kadanoff, L. P. (2001), Turbulent heat flow: Structures and scaling, *Phys. Today*, *54*, 34–38.

Kageyama, A., and T. Sato (1997), Generation mechanism of a dipole field by a magnetohydrodynamic dynamo, *Phys. Rev. E*, *55*, 4617–4626.

Krause, F., and K.-H. Rädler (1980), *Mean-Field, Magnetohydrodynamics and Dynamo Theory*, Elsevier, New York.
Kuang, W., and J. Bloxham (1997), An Earth-like numerical dynamo model, *Nature*, *389*, 371–374.
Labrosse, S. (2002), Hotspots, mantle plumes and core heat loss, *Earth Planet. Sci. Lett.*, *199*, 147–156.
Labrosse, S., J.-P. Poirier, and J.-L. Le Mouël (1997), On cooling of the Earth's core, *Phys. Earth Planet. Inter.*, *99*, 1–17.
Le Huy, M., M. Alexandrescu, J.-L. Le Mouël, and A. Pais (2000), Time evolution of the fluid flow at the top of the core, geomagnetic jerks, *Earth Planet Space*, *52*, 163–173.
Le Mouël, J.-L., C. J. Allègre, and C. Narteau (1997), Multiple scale dynamo, *Proc. Natl. Acad. Sci. U.S.A.*, *94*, 5510–5514.
Macmillan, S. (1996), A geomagnetic jerk for the early 1990's, *Earth Planet. Sci. Lett.*, *137*, 189–192.
Merrill, R. T., M. W. McElhinny, and P. L. McFadden (1996), *The Magnetic Field of the Earth*, *Int. Geophys. Ser.*, vol. 63, Springer, New York.
Moffatt, H. K. (1978), *Magnetic Field Generation in Electrically Conducting Fluids*, Cambridge Univ. Press, New York.
Moffatt, H. K., and D. E. Loper (1994), The magnetostrophic rise of a buoyant parcel in the Earth's core, *Geophys. J. Int.*, *117*, 394–402.
Narteau, C., E. M. Blanter, J.-L. Le Mouël, M. G. Shnirman, and C. J. Allègre (2000), Reversals sequences in a multiple scale dynamo mechanism, *Phys. Earth Planet. Inter.*, *120*, 271–287.
Niemela, J. J., L. Skrnek, K. R. Sreenivasan, and R. J. Donnelly (2000), Turbulent convection at very high Rayleigh numbers, *Nature*, *404*, 837–840.
Olson, P., U. R. Christensen, and G. A. Glatzmaier (1999), Numerical modeling of the geodynamo: Mechanisms of field generation and equilibration, *J. Geophys. Res.*, *104*, 10,383–10,404.
Pouquet, A., and G. Patterson (1978), Numerical simulation of helical magnetohydrodynamic turbulence, *Fluid Mech.*, *85*, 305–323.
Quidelleur, X. (2003), The age and duration of the Matuyama-Brunhes transition from new K-Ar data from La Palma (Canari islands) and revisited $^{40}Ar/^{39}Ar$ ages, *Earth Planet. Sci. Lett.*, *208*, 149–163.
Rikitake, T. (1958), Oscillations of a system of disk dynamos, *Proc. Cambridge Philos. Soc.*, *54*, 89–105.
Roberts, P. H., and S. Scott (1965), On analysis of the secular variation. 1. A hydromagnetic constraint: Theory, *J. Geomagn. Geoelectr.*, *17*, 137–151.
Sreenivasan, K. R., A. Berhadskii, and J. J. Niemela (2002), Mean wind reversal in thermal convection, *Phys. Rev. E*, *65*, (5 Pt 2):056306-056316.
Tilgner, A. (2000), Towards experimental fluid dynamos, *Phys. Earth Planet. Inter.*, *117*, 171–177.
Valet, J. (2003), Time variations in geomagnetic intensity, *Rev. Geophys.*, *41*(1), 1004, doi:10.1029/2001RG000104.
Valet, J.-P., and L. Meynadier (1993), Geomagnetic field intensity and reversals during the past four million year, *Nature*, *366*, 234–238.
Wolfram, S. (1986), *Theory and application of cellular automata*, World Sci., Hackensack, N. J.
Zhang, K., and G. Schubert (2000), Magnetohydrodynamics in rapidly rotating spherical systems, *Annu. Rev. Fluid Mech.*, *32*, 409–443.

J. L. Le Mouël and C. Narteau, Laboratoire de Géomagnétisme, Institut de Physique du Globe de Paris, 4, Place Jussieu, F-75252 Paris Cedex 05, France. (lemouel@ipgp.jussieu.fr; narteau@ipgp.jussieu.fr)